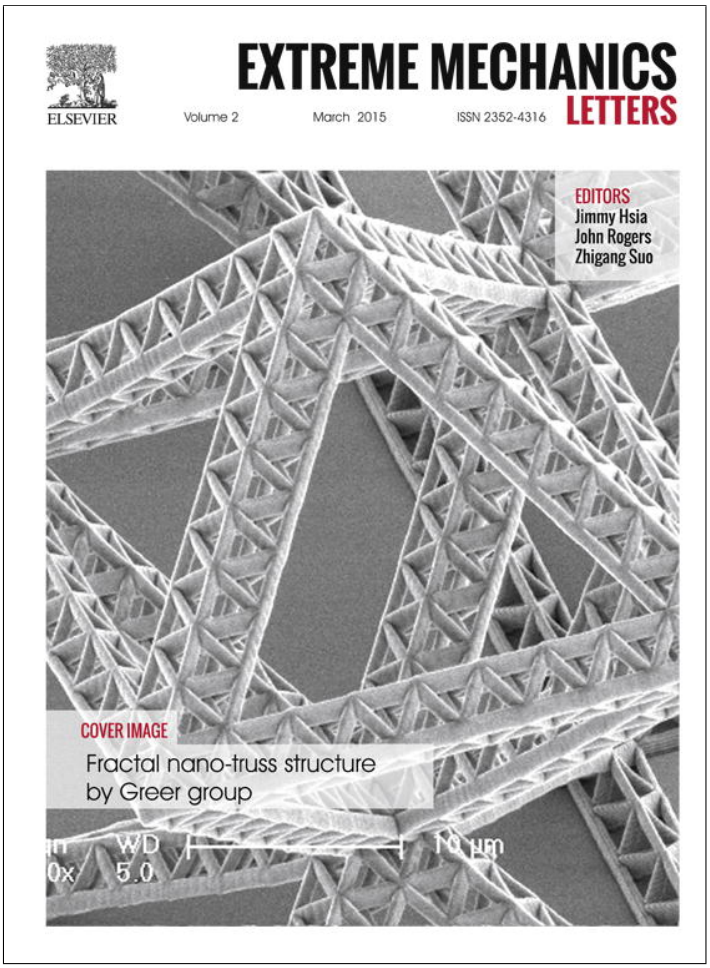

Extreme Mechanics Letters 2 (2015) 28–36

Contents lists available at ScienceDirect

Extreme Mechanics Letters

journal homepage: www.elsevier.com/locate/eml

Ultrasensitive self-powered pressure sensing system

Jianjun Luo [a,1], Feng Ru Fan [a,b,1], Tao Zhou [a], Wei Tang [a], Fei Xue [a], Zhong Lin Wang [a,c,*]

[a] Beijing Institute of Nanoenergy and Nanosystems, Chinese Academy of Science, Beijing 100083, China

[b] Collaborative Innovation Center of Chemistry for Energy Materials, College of Chemistry and Chemical Engineering, Xiamen University, Xiamen 361005, China

[c] School of Material Science and Engineering, Georgia Institute of Technology, Atlanta, GA 30332, USA

ARTICLE INFO

Article history:
Received 26 December 2014
Received in revised form 19 January 2015
Accepted 19 January 2015
Available online 24 January 2015

Keywords:
Self-powered electronics
Pressure sensors
Triboelectric nanogenerator
Sensor integrations
Portable electronics

ABSTRACT

Portable and flexible pressure sensors with highly sensitive and small size have great potential applications in areas such as wearable electronics, environmental monitoring, and medical equipment. Here, we demonstrate an integrated self-powered pressure sensing system made of a passive resistive pressure sensor and a triboelectric nanogenerator. Based on wrinkled and flexible polydimethylsiloxane films, the whole device is of sandwich structure with ultrahigh sensitivity to pressure (204.4 kPa^{-1}), which is more than one order of magnitude higher than all previously reported flexible pressure sensors. And our system exhibits a very low detection limit, rapid response time, and long-term stability. In addition, we built a self-powered, portable visualization system for semi-quantitative analysis of pressure, which can directly convert a pressure information to visual display.

1. Introduction

Highly sensitive, cost-effective, flexible and portable pressure sensors hold an essential position in the development of artificial sensing system. So far, pressure sensors have been reported based on various detection mechanisms, such as resistive [1–9], capacitive [10–12], piezoelectric [13–15], optical [16,17], and triboelectric [18,19]. Among these, resistive pressure sensor (resis-sensor) is used more frequently due to its significant advantages of high sensitivity and rapid response. And it has an excellent performance in monitoring continuous pressure. A common drawback of this type of sensors is that a power source is required for their operation. Most recently, the triboelectric nanogenerator (TENG) [20] has been invented as a promising energy harvesting technology and used for self-powered pressure sensing [18,19]. Even more enticing, TENG operates as a sensor using the electric signal generated by itself without applying an external power source, named as active sensor [21]. This kind of active pressure sensor is very sensitive to the pulse pressure. Moreover, it can be easily assembled into a sensor array for self-powered positioning and imaging [19,22–25], although its sensitivity needs to be further improved. With the development of microelectronics and nanotechnology, the power consumption of the resistive pressure sensors gradually reduce, which is beneficial to be powered by energy-harvesting devices [8], such as TENG. Therefore, it might be a feasible way to overcome the shortcomings of these two kinds of pressure sensors through integrating the resis-sensor and TENG into a single device.

In recent years, owing to its simplicity, cost-effectiveness, flexibility, stretchability, and the ability to be patterned in large areas, surface wrinkling on polydimethylsiloxane (PDMS) has received special attention as a key technology for various future applications, such as optical switching devices [26,27], tunable diffraction gratings [28–30], tunable microfluidics [31,32], microcontact printing masters [33,34], and flexible electronic devices [35,36]. Additionally, it has been proven that the

* Corresponding author at: School of Material Science and Engineering, Georgia Institute of Technology, Atlanta, GA 30332, USA.
E-mail address: zlwang@gatech.edu (Z.L. Wang).

[1] J.L. and F.R.F. contributed equally in this work.

http://dx.doi.org/10.1016/j.eml.2015.01.008
2352-4316/

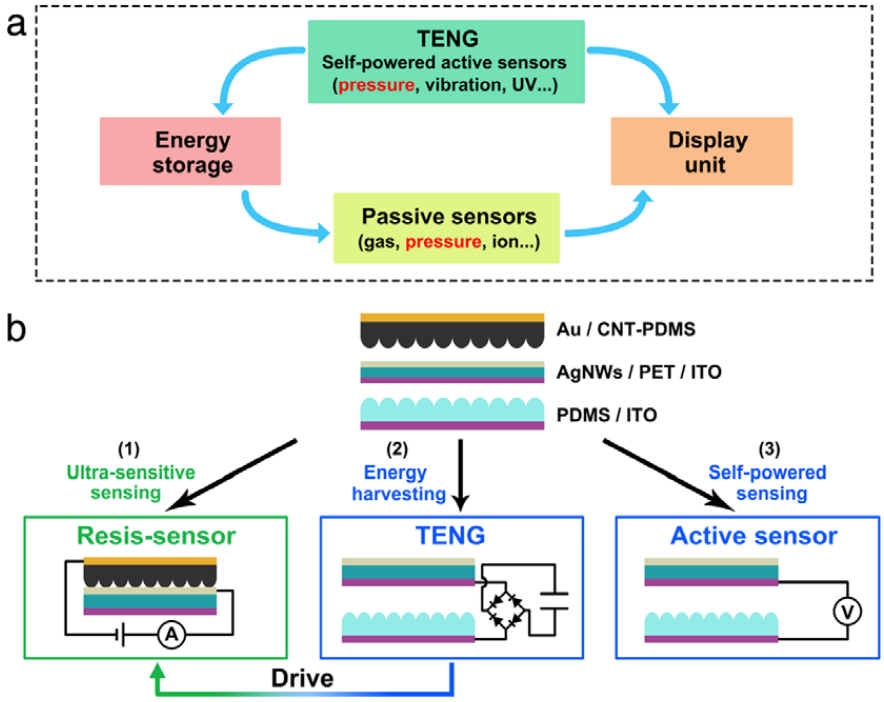

Fig. 1. Schematic diagram of the integrated self-powered sensing system. (a) The integrated self-powered sensing system composed of four parts: TENG, energy storage unit, sensors and display unit. (b) A typical case of self-powered pressure sensing system through the combination of TENG and passive resistive pressure sensor together.

microstructured PDMS can apparently improve the performance of TENGs and flexible pressure sensors [7,10,12,18]. Despite the superior properties of the wrinkled PDMS, to date, it has not yet been used in designing TENGs and flexible pressure sensors.

Here, based on the wrinkled and flexible structure, we devised an ultrasensitive self-powered pressure sensing system, by innovatively integrated the resis-sensor and TENG into a signal device. The wrinkled PDMS employed in the present work effectively improves the electrical output performance of the TENG and the sensitivity of pressure sensors. The whole sensing system exhibits excellent performances of ultra-high sensitivity, very low detection limit, rapid response time, and long-term stability. Combining a display unit, we further built a portable visualization pressure sensing system, which is able to convert the pressure information to visual display directly. We anticipate that this self-powered sensing system could be expanded to other types of self-powered sensors, such as gas sensor, ion sensor, biosensor, and multifunctional sensing might be realized. This work greatly promotes the development of self-powered system, and lays a solid foundation for establishing the future self-powered sensing network.

2. Result and discussion

Concept of the self-powered sensing system. The concept of our integrated self-powered sensing system is illustrated in Fig. 1(a). Firstly, the TENG can be used as self-powered active sensors. In the same time, it harvests different kinds of energy from the environment and stores it in the energy storage unit. Then the collected energy is used to drive the other passive sensor. These two kinds of sensors can work simultaneously and complementarily. The magnitude of detection parameters will be revealed in the display unit. Fig. 1(b) shows a typical example of our self-powered sensing system through the combination of active triboelectric pressure sensor and passive resistive pressure sensor together. The basic working principle of this system is composed of three modes: (1) the upper part is the ultra-sensitive resis-sensor with low operating voltage, which is suitable for continuous monitoring of pressures. But it can work only under the drive of a power source. (2) The lower part is a high-performance TENG for harvesting the environmental energy, and this generating power can be used to drive the resis-sensor. (3) The TENG can be used as a self-powered active pressure sensor, which is suitable to detect the pulsing pressure. Note that the AgNWs and ITO electrodes in the middle layer are connected with each other, constructing an integrated electrode, and these two parts share the middle electrode together, which effectively improves the operating facility of the device. With such a sandwich structure, the device can choose to work in proper mode, depending on different requirement.

Fabrication and characterization of the device. Fig. 2(a) illustrates the fabrication process of the ultra-sensitive self-powered pressure sensing system. The wrinkled carbon nanotube-polydimethylsiloxane (CNT-PDMS) and PDMS were fabricated by mechanical stretching the CNT-PDMS and PDMS films, followed by ultraviolet-ozone (UVO) exposure and strain release. Fig. 2(b) and (c) are SEM images (top, and side view, respectively) showing the detailed microstructure of the wrinkled PDMS film constructed with plenty of parallel wrinkles. The wrinkle wavelength is $\sim$30 μm, and the wrinkle amplitude is $\sim$10 μm. The optical microscope image shows the surface topography of the wrinkled PDMS with large area (Fig. S1), indicating that the surface wrinkles are very uniform,

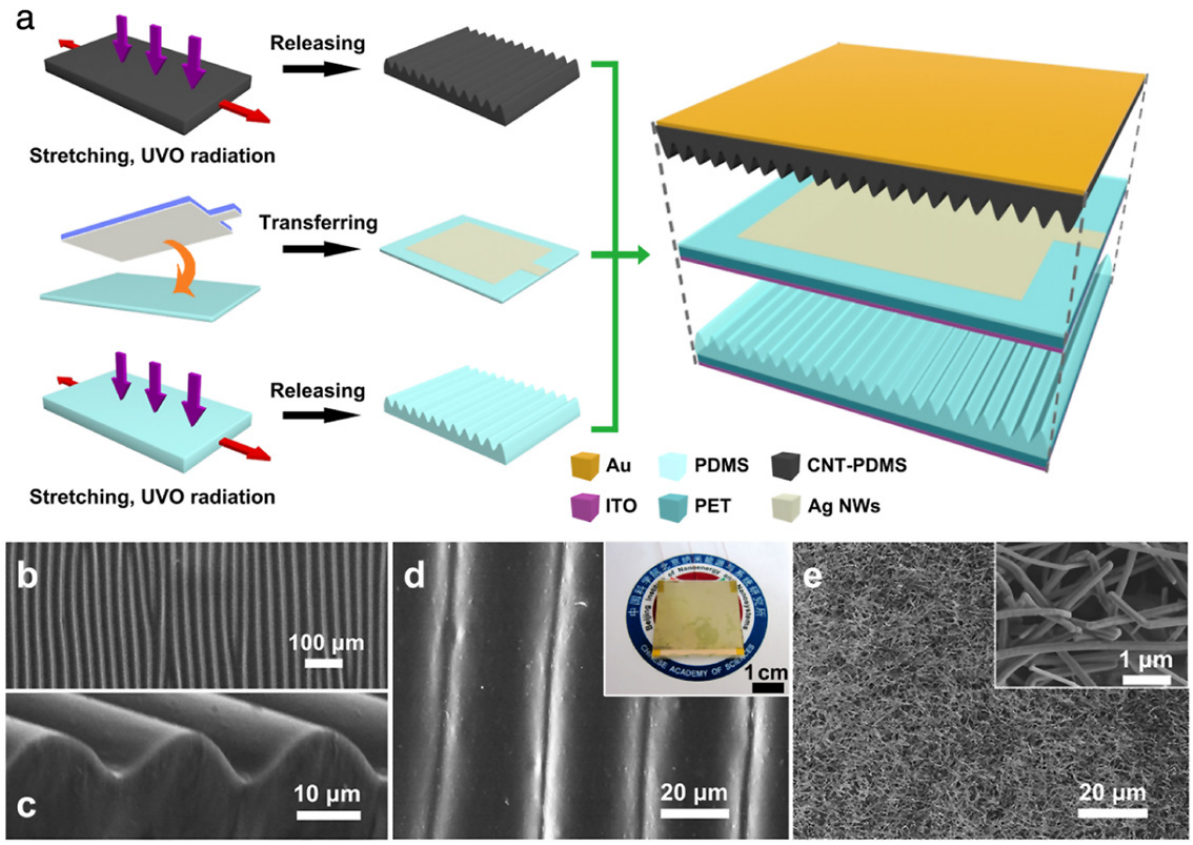

Fig. 2. Fabrication and characterization of the ultrasensitive self-powered pressure sensing system. (a) Schematic of the fabrication of the self-powered pressure sensing system. (b,c) SEM images of the wrinkled PDMS: top (b) and side views (c), respectively. (d) SEM image of the wrinkled CNT-PDMS, inset is the photograph of the dual-mode active pressure sensor. (e) SEM image of AgNWs transferred on PDMS film, inset is a high magnification SEM image of AgNWs.

which is suitable for large-area fabrication. Fig. 2(d) is an SEM image of the wrinkled CNT-PDMS film, revealing regular wrinkled microstructures of the same feature size but rougher surface compared to the wrinkled PDMS. These patterned microstructures with numerous wrinkles can effectively increase the contact sites for the following pressure sensing device. Hence it is beneficial to improve the sensitivity of our system.

Additionally, we used silver nanowires (AgNWs) film and indium tin oxide (ITO) layer as the intermediate two-sided electrode. A thin PDMS film was spin-coated on an ITO-coated PET substrate, then the AgNWs film was transferred from the filter to the cured surface of the PDMS film. Surface structure of the AgNWs/PDMS film is shown in Fig. 2(e). The high magnification SEM image (inset of Fig. 2(e)) shows that the average diameter of AgNWs is 100–200 nm. It can be clearly seen that a part of AgNWs are buried into the PDMS surface and all AgNWs are interconnected with each other forming a three-dimensional (3D) AgNWs network. The AgNWs/PDMS film is flexible with excellent conductivity ($R \sim 3.9\ \Omega$, Fig. S2). Then the processed CNT-PDMS film was deposited with Au on its outer surface as an electrode layer, and placed onto the AgNWs side of the intermediate electrode face to face to form the resis-sensing part. In addition, the processed PDMS film was adhered onto another ITO-coated PET film. And the TENG part was constructed by putting the wrinkled PDMS/PET/ITO film onto the middle ITO electrode face to face, with a PDMS spacer layer between the two triboelectric surfaces. The size of the fabricated device is 3 cm × 3 cm with a sandwich structure (inset of Fig. 2(d)).

Sensing mechanism and response of the resis-sensor. The sensing mechanism of the resis-sensor is due to pressure-dependent change in effective contact area between wrinkled CNT-PDMS and 3D structured AgNWs thin films. Compared to a bulk rigid planar mental, 3D structured AgNWs thin film has large specific surface area and excellent conductivity. Furthermore, the elasticity of PDMS facilitates the contact between these two films, imparting ultra-high sensitivity and reproducible sensing characteristics to our sensor. When applying an external pressure, the pressure-induced deformation increased the contact area of the wrinkled CNT-PDMS and 3D AgNWs thin films. This would cause the sensor to experience a decrease in resistance, leading to an increase in current in a constant voltage (0.1 V). When the external pressure was removed, the two films recovered to their original shapes. This leads to a decrease of contact area between the two films, therefore, causing a decrease of the current. Note that the sensor operating voltage of 0.1 V is sufficiently low to allow for powering by TENGs, thus enabling the integration of self-powered sensing system.

To measure the response of the resis-sensor, we designed a home-made system containing a computer-controlled stepping motor and a force sensor (Fig. S3). The resis-sensor was fixed on a flat plate under the force gauge, and cyclic external pressures were applied by a stepping

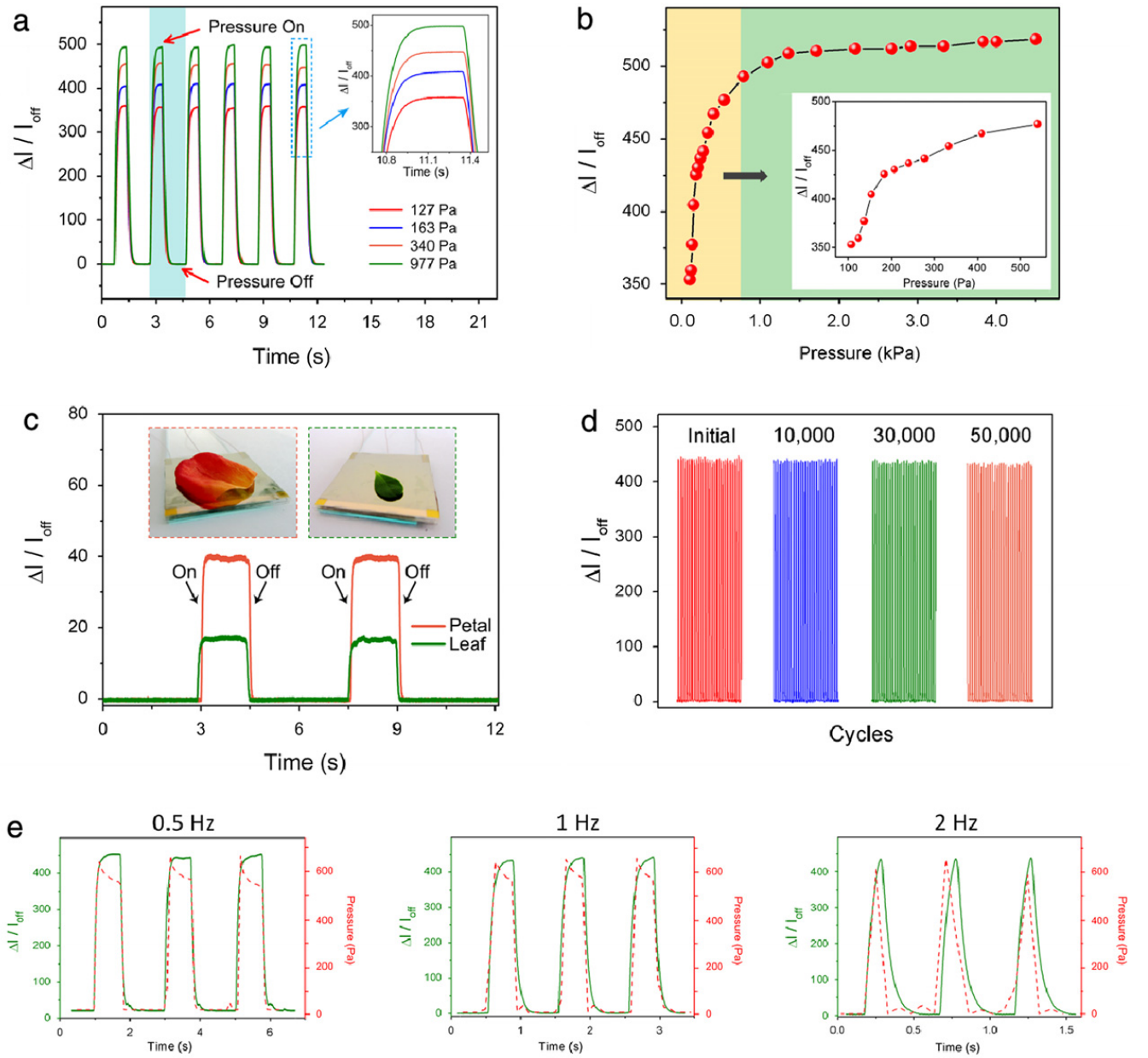

Fig. 3. Electromechanical response of the resis-sensor. (a) The real-time measurement of the relative change of current with cyclic and variable pressures applied on the resis-sensor. The highlighted region indicates one cycle of the pressure loading and unloading process. (b) The summarized relationship and linear fitting between the relative variations of current and the pressure applied on the resis-sensor. (c) The resis-sensor is able to sense the application of very small pressure. Shown is the relative change of current on placing and removing a leaf (20 mg) and a petal (50 mg), respectively. (d) The stability test for pressure sensing of the resis-sensor with continuous loading and unloading a cyclic pressure (250 Pa) for 50,000 cycles, at a frequency of 1 Hz. (e) Plots showing frequency responses at the pressure of 250 Pa: pressure input frequency of 0.5, 1, 2 Hz.

motor. With such a system, external pressures and electrical signals can be recorded simultaneously. Fig. 3(a) is a real-time measurement result of the relative change of current ($\Delta I/I_{off}$) under series of different pressures, and the relationship between $\Delta I/I_{off}$ and magnitude of pressure is plotted in Fig. 3(b). When the applied pressure increased from 107 to 4500 Pa on the sensor, the measured current dramatically increased along with the increase of contact area between the CNT-PDMS wrinkles and AgNWs. The sensitivity S can be defined as:

$$S = \frac{\delta\left(\frac{\Delta I}{I_{off}}\right)}{\delta p} \tag{1}$$

$$\Delta I = I - I_{off} \tag{2}$$

where I is the current when applied pressure on the sensor, and I_{off} is the current of sensor with no pressure, p is the applied pressure. Based on the difference in sensitivity, the plot can be divided into two regions. When the applied pressure was lowered than 800 Pa, the sensitivity (S) is 204.4 kPa^{-1}. To the best of our knowledge, this S in low-pressure regime (<800 Pa) is the highest reported for a flexible pressure sensor, which is significantly higher than those reported in previous literatures. (see Table S1). Fig. 3(c) shows the response of the sensor upon loading–unloading the leaf (20 mg) and petal (50 mg), indicating that the sensor is reliable in detecting minute pressure. The corresponding pressure of the leaf and petal were

0.2 Pa and 0.5 Pa, respectively. Compared to other present flexible pressure sensors reported in the previous literatures (Table S1), our resis-sensor shows a very low detection limit (0.2 Pa).

To further demonstrate the stability of our resis-sensor, a continuous pressure of 250 Pa at a frequency of 1 Hz was applied to the sensor, as shown in Fig. 3(d). Note that the high signal-to-noise ratios (SNR) were well maintained and the current amplitude exhibited negligible changes after 50,000 loading–unloading cycles. The resis-sensor exhibits rapid response time of less than 0.07 s (Fig. S4). The time-resolved response measurement shows that the current waves and the input pressure waves match well under a pressure of 250 Pa at the frequency of 0.5–1 Hz (Fig. 3(e)). When the frequency is up to 2 Hz, a tiny hysteresis can be observed. This might be attributed to the viscoelastic effects of the PDMS films.

Sensing mechanism and response of the TENG as an active sensor. As above, the TENG can be used as an active pressure sensor, and its sensing mechanism is based on coupling effect of contact electrification and electrostatic induction. When an external pressure is applied, the two triboelectric layers are brought into contact with each other. The open-circuit voltage (V_{OC}) will decrease linearly according to equation as followed:

$$V_{OC} = \frac{\sigma \cdot d}{\varepsilon_0} \tag{3}$$

where ε_0 is the permittivity in vacuum, d is the vertical distance between the two layers and σ is the triboelectric charge density, which is considered as constant in this work. Reversely, the V_{OC} reverts to its maximum level when the pressure is fully removed. Considering the mechanism of this active sensor, it is suitable to detect the pulsing pressure.

Fig. 4(a) is the measurement setup for the TENG as an active pressure sensor. In comparison with the resis-sensor, power supply is removed and only volt meter is needed due to the self-powered feature of the TENG. The real-time measurement result of voltage under various pressures is shown in Fig. 4(b). When there is no pressure, the V_{OC} stays at the maximum level ($V_{off} = 150$ V). Once the external pressure is applied, the V_{OC} decreases to a lower level. Fig. 4(c) is the relationship between the relative variations of voltage ($\Delta V/V_{off}$) and the size of pressure ranging from 67 to 2556 Pa. Inset shows the favorable linear relationship of the sensor when the pressure is lower than 400 Pa, which reveals our sensor is reliable for pressure sensing. The sensitivity is defined by:

$$S = \frac{\delta\left(\frac{\Delta V}{V_{off}}\right)}{\delta p} \tag{4}$$

$$\Delta V = V_{off} - V \tag{5}$$

where V_{off} is the voltage of sensor with no pressure, and V is the voltage when applied pressure on the sensor, p is the applied pressure. It can be found that the sensitivity of the sensor is 1.52 kPa^{-1} in the low pressure region, which is much higher than that of high pressure region (0.11 kPa^{-1}). It is noteworthy that this sensitivity is apparently higher than other TENG-based pressure sensors reported previously [18,19]. This is because the electrical output performance of the TENG is greatly improved, using the wrinkled and flexible PDMS.

Furthermore, as shown in Fig. 4(d), the sensor exhibits excellent mechanical robustness and stability under a pressure of 300 Pa at a frequency of 1 Hz, and it can still work properly after 50 000 cycles, with a high SNR. The response time of this sensor is less than 0.09 s (Fig. S5). To examine the delay time of our sensor to external forces, the output voltage signals were compared with the pressure inputs at a frequency of 0.5–2 Hz (Fig. 4(e)). It can be found that the voltage waves were almost the same as the input pressure waves.

Output performance of the TENG. A typical electrical output measurement of the TENG was carried out under a 0.41 Hz external force. As illustrated in Fig. 5(a)–(b), the open circuit voltage and short circuit current of the TENG with a size of 3 cm × 3 cm reach up to 270 V and 21 μA (corresponding to a current density of 2.33 μA cm^{-2}), respectively. Fig. 5(c) shows the dependence of both voltage and current outputs on a series of different resistance (from 10^3 Ω to 1 GΩ). It is clear that the current drops with the increase of the external resistance, while the voltage across the load follows a reversed tendency. Consequently, the effective electrical power of the TENG is closely related to the external load and reaches a maximum value of 1.82 mW at a load resistance of ∼40 MΩ (Fig. 5(d)). The output performance is much higher than our previously reported highly transparent and flexible TENG using flat PDMS films [37]. This might be attributed to the following two factors: (1) the microstructured PDMS has larger effective triboelectric effect than the flat film, which is related to the flexibility and larger surface area of the wrinkled PDMS. (2) UVO treatment can provide large quantities of electric charges to the friction surface.

Self-powered, portable visualization system. Based on the above self-powered pressure sensing system, we further built a portable visualization system, which is constructed with TENG, passive resistive pressure sensor, and display unit. The electric circuit diagram is depicted in Fig. 6(a). This system contains three operating modes, corresponding to different positions (1, 2, 3). When the switch is turned to position 1, the capacitor is connected to the TENG through the rectifier but disconnected from the display. The electrical energy generated by the TENG is stored in the capacitor (22 μF). The charging curve of a capacitor powered by the TENG for 300 s shows a steady increase in the storage charges with the increase of the charging time (middle inset of Fig. 6(b)). Next, the charged capacitor will be used as a power source to drive the resis-sensor by turning the switch to position 2. In this mode, the display will show different bits according to the size of pressure applied to the resis-sensor. Here, to quantify its response, we measured the working curve of the sensor (Fig. 6(b)). The peak current increases to 16 μA when a pressure is applied to the resis-sensor. Then the capacitor is charged to the same state by the TENG. When applying the same magnitude of pressure, the peak current rises up to 16 μA again, indicating that the resis-sensor can work properly even driven by a capacitor.

Besides, the TENG itself can also be used as an active pressure sensor for semi-quantitative pressure sensing

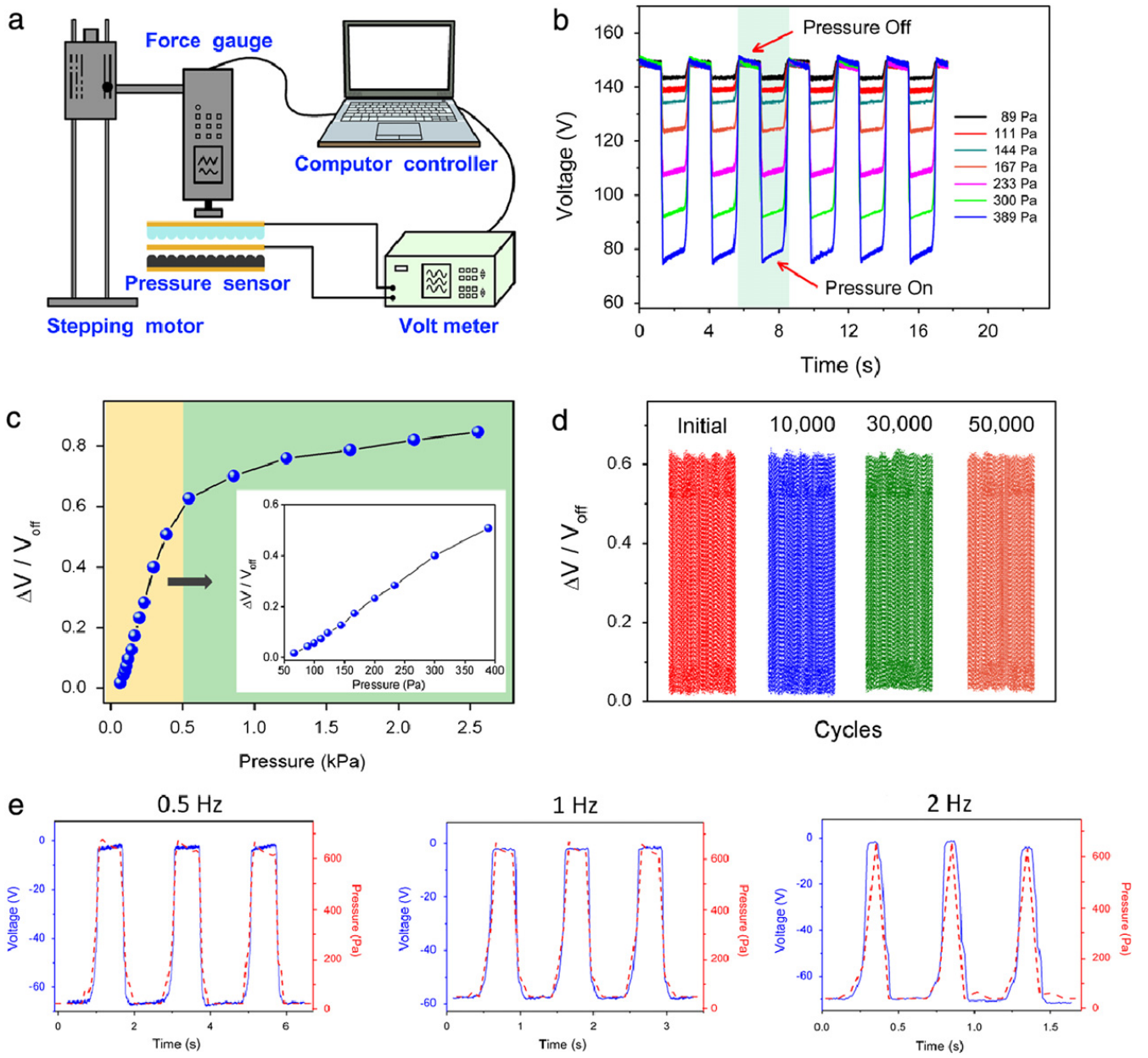

Fig. 4. Electromechanical response of the TENG as an active pressure sensor. (a) Schematic illustration of the experimental setup of the active sensor. (b) The real-time measurement of the voltage with cyclic and variable pressures applied on the active sensor. The highlighted region indicates one cycle of the pressure loading and unloading process. (c) The summarized relationship and linear fitting between the relative variations of voltage and the pressure applied on the active sensor. (d) The stability test for pressure sensing of the active sensor with continuous loading and unloading a cyclic pressure (300 Pa) for 50,000 cycles, at a frequency of 1 Hz. (e) Plots showing frequency responses at the pressure of 300 Pa: pressure input frequency of 0.5, 1, 2 Hz.

while the switch is turned to position 3, using a force gauge to measure the size of pressure (Movie S1). And this visualization system itself can work without any measuring instrument for qualitative purpose (Movie S2). As shown in Fig. 6(c), when a low pressure (less than 200 Pa) is applied to the device, only the first signal of number displays in the LCD screen. Then, with the pressure increases to medium (range from 200 to 600 Pa) and high (larger than 600 Pa) levels, the second and third signals of number in the LCD screen will be visible. Without the need of any other complex apparatus to record and analyze the output signal, this self-powered system can be used to reveal the size of pressure semi-quantitatively and directly. Based on the same principle, the resolution of this sensing system can be further improved by upgrading its integration capabilities. With the cost-effective, portable and simple design, this self-powered visualization system greatly promotes the development of intuitional pressure sensing and might expend to other types of self-powered sensing system.

3. Conclusion

In summary, we have developed a simple, cost-effective method to fabricate an ultrasensitive self-powered pressure sensing system, by innovatively integrating the resis-sensor and the TENG into a single device. With the help of wrinkled and flexible PDMS, our sensing system exhibits multiple excellent performances. The resis-sensor

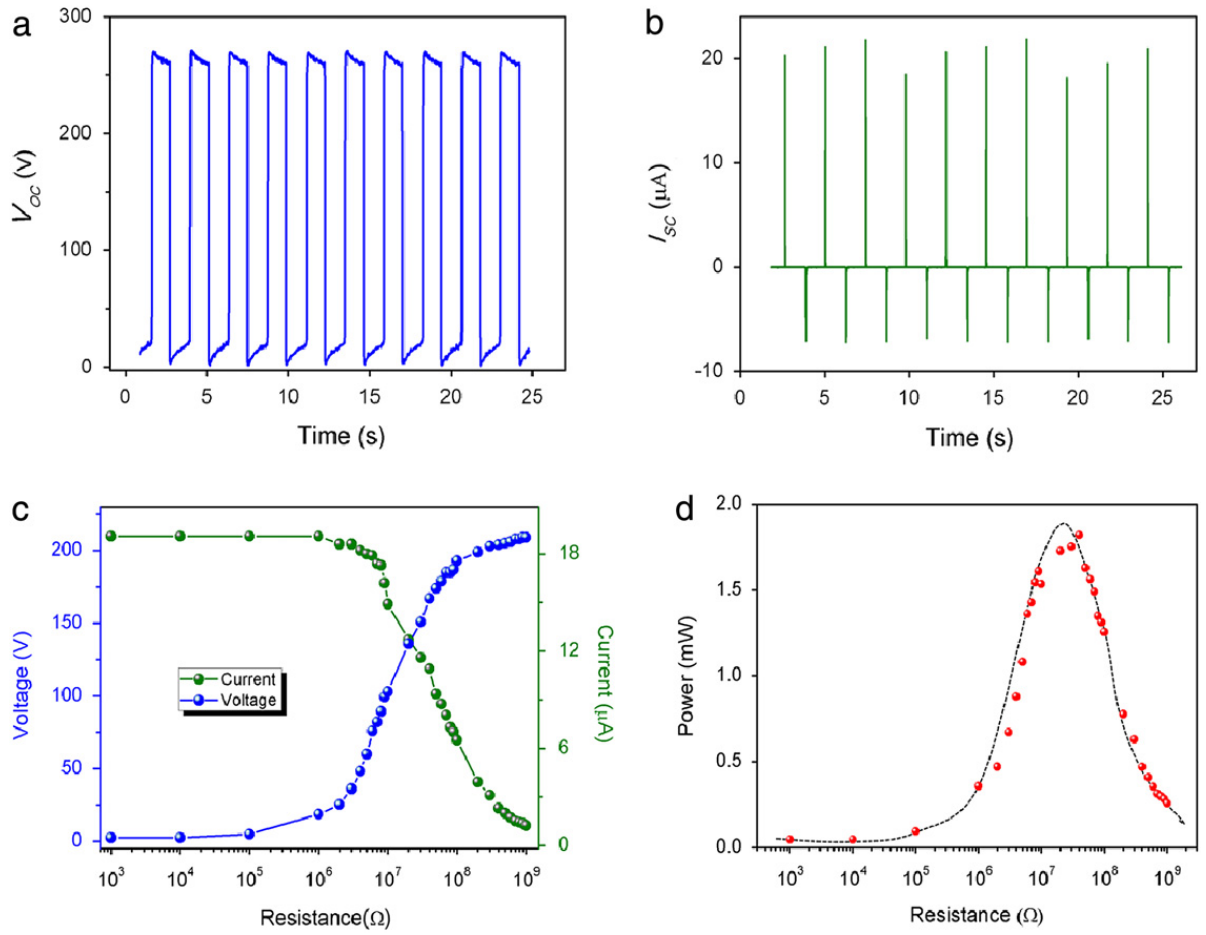

Fig. 5. Output performance characterization of the TENG. (a) Open circuit voltages and (b) Short circuit currents of the TENG. (c), (d) Dependence of the output voltage and current (c) and the effective power output (d) of the TENG on the resistance of external load.

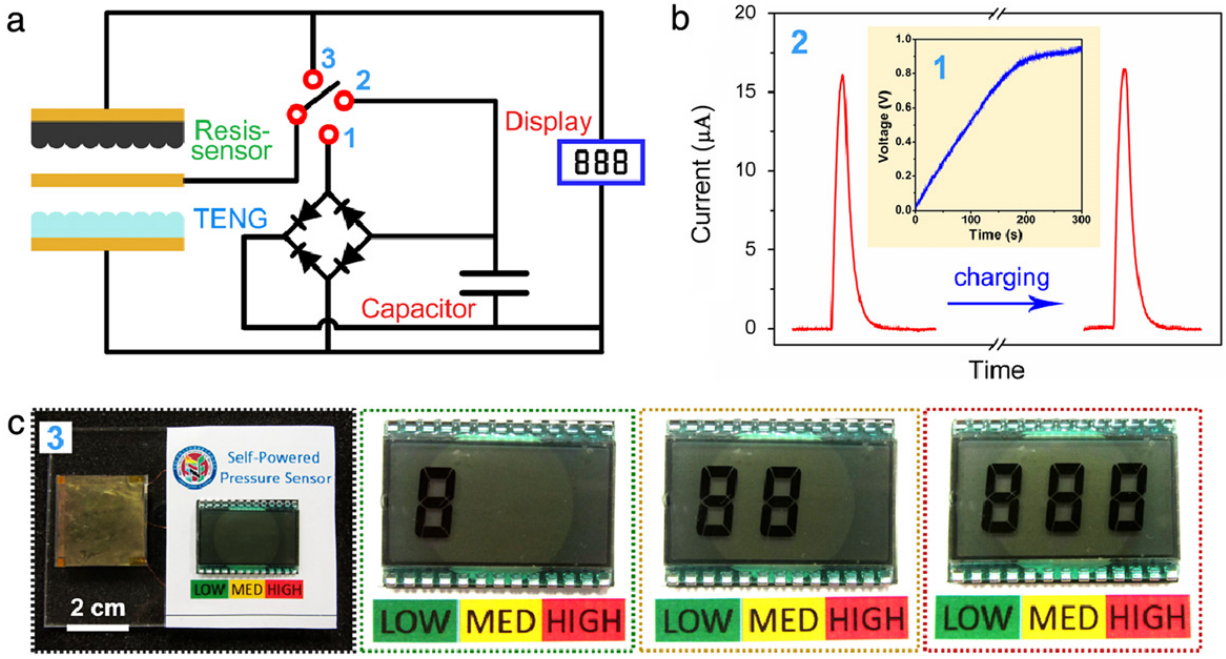

Fig. 6. Demonstration of a self-powered, portable visualization pressure sensing system. (a) Electric circuit diagram of the pressure sensing system. (b) The working curve of the resis-sensor driven by the capacitor, middle inset is the charging curve of the capacitor powered by the TENG. (c) Photographs of the self-powered, portable visualization sensing system at different pressure.

demonstrates ultra-high sensitivity (204.37 kPa^{-1}) in the low-pressure regime (<800 Pa), very low detection limit (0.2 Pa), and rapid response time (<0.07 s). Remarkably, this sensitivity is the highest value among any reported flexible pressure sensors. By contrast, when using the TENG as an active pressure sensor, it shows a high sensitivity (1.52 kPa^{-1}) and fast response time (<0.09 s). Both types of sensors have excellent performances of long-term stability (beyond 50,000 cycles) and low response delay between electric signals and mechanical signals at low frequency (0.5–2 Hz). When using the TENG as an energy harvester, it has an excellent output performance. A very large output of up to 270 V and 21 μA at a current density of 2.33 μA cm^{-2}, and an effective electrical power up to 1.82 mW (2.02 W/m^2) at a load resistance of ∼40 MΩ were obtained. Moreover, a self-powered, portable visualization sensing system was built for semi-quantitative detection of pressure directly. Further optimization of the system will focus on the features of miniaturization, transparent and wearable. We also believe that this self-powered visualized sensing system could be expanded to other types of self-powered sensors, and multifunctional sensing might be realized simultaneously and complementarily.

Experimental section

Preparation of the wrinkled CNT-PDMS film. To fabricate of the precured 5 wt% CNT-PDMS film, single-walled nanotubes (SWNT, CHANGXIANG Inc.) were dispersed by ultrasonic in chloroform for 8 h. The dispersed CNT solution was completely mixed with PDMS base (Sylgard 184, Tow Corning) using a vortex mixer. Chloroform was subsequently removed by evaporation for 12 h at 90 °C on an oven. Then PDMS curing agent (1:10 ratio for curing agent to base) and hexane were added to the dried CNT-PDMS (at a ratio of 1 mL of hexane for each 600 mg of PDMS) and mixed with a vortex mixer for 10 min. For the fabrication of wrinkled CNT-PDMS film, the fluid mixture was spin-coated (500 rpm) onto a silicon wafer and thermally cured at 80 °C for 2 h. The fully cured composite film (∼200 μm) was uniaxially stretched with a prestrain value of 40% before being placed in the UVO chamber (BZS250GF-TC, HWOTECH Inc.) for 20–30 min. The prestrain was then removed, resulting in a wrinkled structure in the CNT-PDMS surface.

Synthesis of AgNWs. The long AgNWs were synthesized by a multi-steps method, according to the method reported previously with some modification [38]. In the first step, 5.86 g of PVP (Mw: ∼40 000) were dissolved into 190 mL of glycerol and heated at 90 °C in the oven for 2 h. When the solution was cooled down to 50 °C, 1.58 g $AgNO_3$ power was added. Then, 10 mL of glycerol, 59 mg of NaCl and 0.5 mL of H_2O were mixed and added into the above solution. Afterward, the mixed solution was heated up to 210 °C in 25 min under gentle stirring (∼200 rpm). Subsequently, the heat to the solution was removed. In step two, the resulting AgNWs were used as crystal seeds for synthesizing the long AgNWs. Briefly, the whole process was the same as step one, except that 3 mL of seed AgNWs were used in placed of the glycerol/ $NaCl/H_2O$ solution. Finally, the obtained AgNWs solution was transferred into a beaker, followed by adding 200 mL deionized water. After stabilized for one day, upper layer silver nanoparticles (AgNPs) solution was removed and bottom layer sediment (AgNWs) was collected and washed with water twice.

Preparation of the wrinkled PDMS film. For the fabrication of wrinkled PDMS, PDMS base and curing agent were thoroughly mixed in a 10:1 ratio (w/w) and degassed for 30 min. Then the fluid mixture was spin-coated (500 rpm) onto a silicon wafer and thermally cured at 80 °C for 2 h. The fully cured composite film (∼150 μm) was uniaxially stretched with a prestrain value of 40% before being placed in the UVO chamber for 10–20 min. The prestrain was then removed, resulting in a wrinkled structure in the PDMS surface.

Fabrication of the ultrasensitive self-powered pressure sensing system. A wrinkled CNT-PDMS (3 cm × 3 cm) was deposited with Au on its outer surface as electrode layer (Denton Sputter). Then, a fluid mixture of PDMS base and its curing agent (10:1, w/w) was spin-coated (1500 rpm) onto an ITO-coated PET film (3 cm × 3 cm) and semi-cured at 75 °C for 15 min. A filter paper was used to filter the AgNWs suspension and cut by paper knife into 2.5 cm × 2.5 cm piece. Then the AgNWs/paper was brought into contact with the semi-cured PDMS film (∼50 μm) and the AgNWs film was transferred onto the PDMS film. The AgNWs/PDMS/PET/ITO film was fully cured at 80 °C for 2 h. Next, the wrinkled CNT-PDMS film was deposited onto the top surface of AgNWs/PDMS/PET/ITO film to form the upper layer and middle layer, respectively. Then a wrinkled PDMS (3 cm × 3 cm) was adhered on another ITO-coated PET film as the bottom layer. Finally, the wrinkled PDMS surface of the bottom layer was placed onto the middle ITO electrode, and a PDMS spacer layer was inserted at the edges of the middle ITO electrode to separate the two triboelectric surfaces. Finally, the Dual-mode Active Pressure Sensor with sandwich structure was achieved. The effective size of the sensor is 3 cm × 3 cm and the thickness is about 3 mm.

Measurement. SEM images were characterized using a HITACHI SU8020 FE-SEM operated at 5 kV beam voltage. Optical images were taken by a Zeiss Observer Z1 microscope. The computer controlled linear mechanical motor (Linmot Inc.) and force gauge (Handpi Digital force gauge, HP3) were used to apply the external pressure. The Keithley 6514 System Electrometer was used to measure the V_{OC}. The SR570 low noise current amplifier was used to measure the I_{SC}. Keithley 2400 was used to supply the constant voltage.

Acknowledgments

This research was supported by the "thousands talents" program for pioneer researcher and his innovation team, China, National Natural Science Foundation of China (Grant No. 51432005), and Beijing City Committee of science and technology project (Z131100006013004, Z131100006013005). The authors would like to thank Weiming Du, Liming Zhang and Chao Yuan for helpful discussions and assistance in experiments.

Conflict of interest

The authors declare no competing financial interest.

Appendix A. Supplementary data

Supplementary material related to this article can be found online at http://dx.doi.org/10.1016/j.eml.2015.01.008.

References

[1] T. Yamada, Y. Hayamizu, Y. Yamamoto, Y. Yomogida, A. Izadi-Najafabadi, D.N. Futaba, K.A. Hata, Stretchable carbon nanotube strain sensor for human-motion detection, Nature Nanotechnol. 6 (2011) 296–301.

[2] C. Pang, G.Y. Lee, T.I. Kim, S.M. Kim, H.N. Kim, S.H. Ahn, K.Y. Suh, A flexible and highly sensitive strain-gauge sensor using reversible interlocking of nanofibres, Nature Mater. 11 (2012) 795–801.

[3] L.J. Pan, A. Chortos, G.H. Yu, Y.Q. Wang, S. Isaacson, R. Allen, Y. Shi, R. Dauskardt, Z.N. Bao, An ultra-sensitive resistive pressure sensor based on hollow-sphere microstructure induced elasticity in conducting polymer film, Nature Commun. 5 (2014) 3002.

[4] S. Gong, W. Schwalb, Y.W. Wang, Y. Chen, Y. Tang, J. Si, B. Shirinzadeh, W.L. Cheng, A wearable and highly sensitive pressure sensor with ultrathin gold nanowires, Nature Commun. 5 (2014) 3132.

[5] J. Park, Y. Lee, J. Hong, M. Ha, Y.D. Jung, H. Lim, S.Y. Kim, H. Ko, Giant tunneling piezoresistance of composite elastomers with interlocked microdome arrays for ultrasensitive and multimodal electronic skins, ACS Nano 5 (2014) 4689–4697.

[6] B.W. Zhu, Z.Q. Niu, H. Wang, W.R. Leow, H. Wang, Y.G. Li, L.Y. Zheng, J. Wei, F.W. Huo, X.D. Chen, Microstructured graphene arrays for highly sensitive flexible tactile sensors, Small 10 (2014) 3625–3631.

[7] X.W. Wang, Y. Gu, Z.P. Xiong, Z. Cui, T. Zhang, Silk-molded flexible, ultrasensitive, and highly stable electronic skin for monitoring human physiological signals, Adv. Mater. 26 (2014) 1336–1342.

[8] C.L. Choong, M.B. Shim, B.S. Lee, S. Jeon, D.S. Ko, T.H. Kang, J. Bae, S.H. Lee, K.E. Byun, J. Im, Highly stretchable resistive pressure sensors using a conductive elastomeric composite on a micropyramid array, Adv. Mater. 26 (2014) 3451–3458.

[9] H.B. Yao, J. Ge, C.F. Wang, X. Wang, W. Hu, Z.J. Zheng, Y. Ni, S.H. Yu, A flexible and highly pressure-sensitive graphene polyurethane sponge based on fractured microstructure design, Adv. Mater. 25 (2013) 6692–6698.

[10] S.C.B. Mannsfeld, B.C.K. Tee, R.M. Stoltenberg, C.V.H.H. Chen, S. Barman, B.V.O. Muir, A.N. Sokolov, C. Reese, Z.N. Bao, Highly sensitive flexible pressure sensors with microstructured rubber dielectric layers, Nature Mater. 9 (2010) 859–864.

[11] D.J. Lipomi, M. Vosgueritchian, B.C.K. Tee, S.L. Hellstrom, J.A. Lee, C.H. Fox, Z.N. Bao, Skin-like pressure and strain sensors based on transparent elastic films of carbon nanotubes, Nature Nanotechnol. 6 (2011) 788–792.

[12] G. Schwartz, B.C.K. Tee, J.G. Mei, A.L. Appleton, D.H. Kim, H.L. Wang, Z.N. Bao, Flexible polymer transistors with high pressure sensitivity for application in electronic skin and health monitoring, Nature Commun. 4 (2013) 1859.

[13] W.Z. Wu, X.N. Wen, Z.L. Wang, Taxel-addressable matrix of vertical-nanowire piezotronic transistors for active and adaptive tactile imaging, Science 340 (2013) 952–957.

[14] D. Mandal, S. Yoon, K.J. Kim, Origin of piezoelectricity in an electrospun poly(vinylidene fluoride-trifluoroethylene) nanofiber web-based nanogenerator and nano-pressure sensor, Macromol. Rapid Commun. 32 (2011) 831–837.

[15] Y.F. Hu, C. Xu, Y. Zhang, L. Lin, R.L. Snyder, Z.L. Wang, A nanogenerator for energy harvesting from a rotating tire and its application as a self-powered pressure/speed sensor, Adv. Mater. 23 (2011) 4068–4071.

[16] M. Ramuz, B.C.K. Tee, J.B.H. Tok, Z.N. Bao, Transparent, optical, pressure-sensitive artificial skin for large-area stretchable electronics, Adv. Mater. 24 (2012) 3223–3227.

[17] S. Yun, S. Park, B. Park, Y. Kim, S.K. Park, S. Nam, K.U. Kyung, Polymer-waveguide-based flexible tactile sensor array for dynamic response, Adv. Mater. 26 (2014) 4474–4480.

[18] F.R. Fan, L. Lin, G. Zhu, W.Z. Wu, R. Zhang, Z.L. Wang, Transparent triboelectric nanogenerators and self-powered pressure sensors based on micropatterned plastic films, Nano Lett. 12 (2012) 3109–3114.

[19] L. Lin, Y.N. Xie, S.H. Wang, W.Z. Wu, S.M. Niu, X.N Wen, Z.L. Wang, Triboelectric active sensor array for self-powered static and dynamic pressure detection and tactile imaging, ACS Nano 7 (2013) 8266–8274.

[20] F.R. Fan, Z.Q. Tian, Z.L. Wang, Flexible triboelectric generator, Nano Energy 1 (2012) 328–334.

[21] Z.L. Wang, Triboelectric nanogenerators as new energy technology for self-powered systems and as active mechanical and chemical sensors, ACS Nano 7 (2013) 9533–9557.

[22] Y. Yang, H.L. Zhang, Z.H. Lin, Y.S. Zhou, Q.S. Jing, Y.J. Su, J. Yang, J. Chen, C.G. Hu, Z.L. Wang, Human skin based triboelectric nanogenerators for harvesting biomechanical energy and as self- powered active tactile sensor system, ACS Nano 7 (2013) 9213–9222.

[23] C.B. Han, C. Zhang, X.H. Li, L.M. Zhang, T. Zhou, W.G. Hu, Z.L. Wang, Self-powered velocity and trajectory tracking sensor array made of planar triboelectric nanogenerator pixels, Nano Energy 9 (2014) 325–333.

[24] S.H. Wang, L. Lin, Z.L. Wang, Triboelectric nanogenerators as self-powered active sensors, Nano Energy 11 (2015) 436–462.

[25] M.D. Han, X.S. Zhang, X.M. Sun, B. Meng, W. Liu, H.X. Zhang, Magnetic-assisted triboelectric nanogenerators as self-powered visualized omnidirectional tilt sensing system, Sci. Rep. 4 (2014) 4811.

[26] E.P. Chan, A.J. Crosby, Fabricating microlens arrays by surface wrinkling, Adv. Mater. 18 (2006) 3238–3242.

[27] H.S. Kim, A.J. Crosby, Solvent-responsive surface via wrinkling instability, Adv. Mater. 23 (2011) 4188–4192.

[28] N. Bowden, W.T.S. Huck, K.E. Paul, G.M. Whitesides, The controlled formation of ordered, sinusoidal structures by plasma oxidation of an elastomeric polymer, Appl. Phys. Lett. 75 (1999) 2557–2559.

[29] C.M. Stafford, C. Harrison, K.L. Beers, A. Karim, E.J. Amis, M.R. Vanlandingham, H.C. Kim, W. Volksen, R.D. Miller, E.E. Simonyi, A buckling-based metrology for measuring the elastic moduli of polymeric thin films, Nature Mater. 3 (2004) 545–550.

[30] C. Harrison, C.M. Stafford, W.H. Zhang, A. Karim, Sinusoidal phase grating created by a tunably buckled surface, Appl. Phys. Lett. 85 (2004) 4016–4018.

[31] K. Khare, J.H. Zhou, S. Yang, Tunable open-channel microfluidics on soft poly(dimethylsiloxane) (PDMS) substrates with sinusoidal grooves, Langmuir 25 (2009) 12794–12799.

[32] K. Efimenko, M. Rackaitis, E. Manias, A. Vaziri, L. Mahadevan, J. Genzer, Nested self-similar wrinkling patterns in skins, Nature Mater. 4 (2005) 293–297.

[33] M. Pretzl, A. Schweikart, C. Hanske, A. Chiche, U. Zettl, A. Horn, A. Boker, A. Fery, A lithography-free pathway for chemical microstructuring of macromolecules from aqueous solution based on wrinkling, Langmuir 24 (2008) 12748–12753.

[34] S.G. Lee, H. Kim, H.H. Choi, H. Bong, Y.D. Park, W.H. Lee, K. Cho, Evaporation-induced self-alignment and transfer of semiconductor nanowires by wrinkled elastomeric templates, Adv. Mater. 25 (2013) 2162–2166.

[35] D.Y. Khang, H.Q. Jiang, Y. Huang, J.A. Rogers, A stretchable form of single-crystal silicon for high-performance electronics on rubber substrates, Science 311 (2006) 208–212.

[36] M. Melzer, D. Makarov, A. Calvimontes, D. Karnaushenko, S. Baunack, R. Kaltofen, Y.F. Mei, O.G. Schmidt, Stretchable magnetoelectronics, Nano Lett. 11 (2011) 2522–2526.

[37] F.R. Fan, J.J. Luo, W. Tang, C.Y. Li, C.P. Zhang, Z.Q. Tian, Z.L. Wang, Highly transparent and flexible triboelectric nanogenerators: performance improvements and fundamental mechanisms, J. Mater. Chem. A 2 (2014) 13219–13225.

[38] C. Yang, H.W. Gu, W. Lin, M.M. Yuen, C.P. Wong, M.Y. Xiong, B. Gao, Silver nanowires: from scalable synthesis to recyclable foldable electronics, Adv. Mater. 23 (2011) 3052–3056.